Self-trapped states and the related luminescence in PbCl$_2$ crystals

Masanobu Iwanaga

Graduate School of Human and Environmental Studies, Kyoto University, Kyoto 606-8501, Japan

Masanobu Shirai and Koichiro Tanaka

Department of Physics, Graduate School of Science, Kyoto University, Kyoto 606-8502, Japan

Tetsusuke Hayashi

Faculty of Integrated Human Studies, Kyoto University, Kyoto 606-8501, Japan
(Dated: February 1, 2008)

We have comprehensively investigated localized states of photoinduced electron-hole pairs with electron-spin-resonance technique and photoluminescence (PL) in a wide temperature range of 5–200 K. At low temperatures below 70 K, holes localize on Pb^{2+} ions and form self-trapping hole centers of Pb^{3+}. The holes transfer to other trapping centers above 70 K. On the other hand, electrons localize on two Pb^{2+} ions at higher than 50 From the thermal stability of the localized s 2.50 eV is closely related to the self-trapped l

I. INTRODUCTION

Electronic excited states relax into self-trapped (ST) states in solids where electrons strongly interact wi acoustic phonons.[1] The structure of ST states h been extensively examined with electron-spin-resonan (ESR) technique in ionic crystals.[2,3] The annihilation the ST states often induces photons due to electron-ho (e-h) recombination via electric dipole transition. Ther fore, luminescence study is another effective techniqu to investigate the ST states in high-efficient luminesce materials. Comprehensive study with ESR technique ar luminescence spectroscopy is often powerful enough clarify the ST states and the correlation with lumine cence.

Localized states of excited electrons and holes in PbC crystals have been studied with ESR technique for th past few decades. In the early stage around 1970, th localized states induced by ultraviolet (UV) light irrad ation at 80 K were observed around $g \approx 2$ (Refs. 4,5,6 Figure 1 shows ESR signals photoinduced at 80 K; a s of five resonances around $g \approx 2$ was named as "A si nal"[5] and is enlarged in the inset. In addition, the ES signals after x-ray irradiation at 10 K were also reporte around $g \approx 2$, and were named as "B signal" and " signal."[5] Though some trials were performed,[4,5,6] the l calized state responsible for the A signal has been di putable[7] and the origins of the B and C signals have n been identified yet. The next advance was reported l Nistor *et al.*[8] and Hirota *et al.*[9] in 1993; self-trapped ele trons (STEL's) induced by x-ray[8] and γ-ray[9] irradiation at 80 K were observed and found to be dimer-molecular Pb$_2{}^{3+}$ centers. The ESR spectrum of Pb$_2{}^{3+}$ is also pre sented in Fig. 1.

Localized states in PbF$_2$ (Ref. 10) and PbBr$_2$ (Ref. 11) have been revealed with ESR technique. In PbF$_2$, only holes get self-trapped and form Pb^{3+} centers.[10] On the
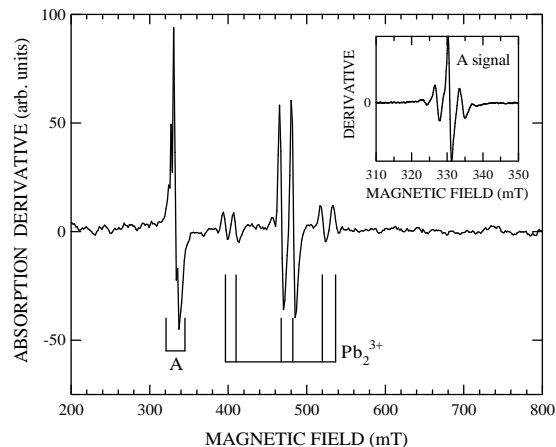

FIG. 1: Typical ESR spectrum measured at 9 K after pho toirrdiation at 80 K; the light source is described in Sec. II. The inset enlarges "A signal" around 330 mT. Microwave fre quency was 9.400 GHz. Magnetic field vector **B** was in bc plane; the angle between the **B** and the b axis was 10°.

other hand, both electrons and holes get self-trapped in PbBr$_2$, and form electron centers of Pb$_2{}^{3+}$ and hole cen ters of Br$_2{}^-$, respectively.[11] The configurations of self trapped holes (STH's) are different between PbF$_2$ and PbBr$_2$. The difference is qualitatively explained by the components at the top of the valence bands; the 6s states of Pb^{2+} are the main component in PbF$_2$, while the 4p states of Br$^-$ mainly constitute the valence band in PbBr$_2$ (Ref. 12). According to the cluster calculation[12] for PbCl$_2$, the top of the valence band is composed of about half-and-half Pb^{2+} (6s) and Cl$^-$ (3p). Therefore, the structure of localized hole centers in PbCl$_2$ is signif icant to clarify the relation of hole-relaxation dynamics with the electronic-band structure in PbCl$_2$ and to un

derstand the relation in lead halides comprehensively.

Luminescence in $PbCl_2$ has been studied in parallel to the ESR. The intense photoluminescence (PL) at low temperatures below 10 K was classified to UV-PL band at 3.8 eV, blue-PL band at 2.8 eV, and blue-green (BG) PL band at 2.5 eV.[5,13,14] The UV-PL and the blue-PL bands are mainly induced under one-photon excitation into the exciton band, and the BG-PL band is dominantly induced under excitation into the energy region higher than the lowest exciton.[39] As the origins of the UV-PL band at 3.76 eV and the blue-PL band at 2.88 eV, the self-trapped excitons (STE's) with the configuration of (Pb^+ + hole) were proposed, and the origin of the BG-PL band was attributed to the STE's of (Pb_2^{3+} + hole).[15,16,17] The models claim that the lowest excitons and free e-h pairs relax into different localized states. However, the Pb^+ centers in $PbCl_2$ have not been reported. Another interpretation on the PL bands was recently proposed;[18] it declares that the UV-PL and blue-PL bands come from the STE's of (Pb_2^{3+} + hole) and the BG-PL band originates from the tunneling recombination of the pairs of a STEL of Pb_2^{3+} and a STH of Cl_2^-. On the other hand, another PL study[19] has shown that the PL below 10 K under two-photon excitation into the exciton band is dominantly composed of the BG-PL band, and the intensity of the UV-PL band heavily saturates such that $I_{UV} \propto I^{0.6}$ where I is intensity of incident light. The results imply that, under the bulk excitation like two-photon excitation, the relaxed states of e-h pairs are independent of the excitation energy and yield the BG-PL band. Consequently, it is possible enough to explain that the lowest excitons created under one-photon excitation are captured by surface defects and result in the UV-PL and the blue-PL bands. Thus, the origins of PL bands are still disputable.

Excitons in $PbBr_2$ crystals, which belong to the same crystallographic group[20] with $PbCl_2$ and have similar electronic-band structures,[12,21,22,23] undergo uncommon relaxation;[24] they spontaneously dissociate and relax into spatially-separated STEL's and STH's. The recent ESR study[11] supports the relaxed state of excitons structurally. A similar relaxation in $PbCl_2$ has been pointed out,[19] but the structures of the localized states have not been explored fully as already described.

We have comprehensively examined the localized states of photoinduced e-h pairs and PL properties in a wide temperature range of 5–200 K. As a result, the localized states of holes at low temperatures below 70 K have been found to form STH centers of Pb^{3+}; the structure of STH's is different from that inferred from the ESR spectrum at 80 K as shown in Fig. 1 and from the recent study on $PbBr_2$ (Ref. 11). We present the low-temperature ESR signals photoinduced below 10 K in Sec. III A and the PL properties in Sec. III B. The STH's are analyzed with spin Hamiltonian in Sec. IV A. We discuss the correlation between ESR signals and PL in Sec. IV B, the origin of the A signal in Sec. IV C, and the relaxation dynamics of e-h pairs in comparison with
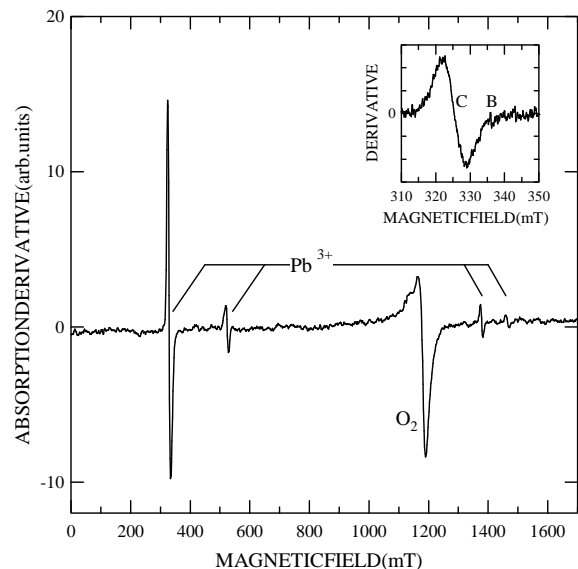

FIG. 2: Typical ESR spectrum measured at 7 K after photoirrdiation at 6 K. The inset enlarges the signals around 330 mT. Microwave frequency was 9.400 GHz. Magnetic field vector $\mathbf{B}$ was in the bc plane; the angle between the $\mathbf{B}$ and the b axis was 40°. Descriptions for Pb^{3+}, O_2, B, and C are given in Sec. III A.

$PbBr_2$ in Sec. IV D.

II.   EXPERIMENTS

Single crystal of $PbCl_2$ was grown with the Bridgman technique from 99.999% powder. The crystal of orthorhombic D_{2h}^{16} (Ref. 20) was cut in the size of $3 \times 3 \times 3$ mm^3 along the right-angled crystallographic a, b, and c axes.

The sample was photoirradiated with the second harmonics (pulsed 120-fs-width, 1-kHz, and 3.10-eV light) generated from a regeneratively amplified Ti:sapphire laser; average power of the incident light was about 20 mW/cm^2 on the sample surface. The incident photons induce two-photon interband transition, create e-h pairs almost uniformly in the crystal, and produce measurable ESR signals within one minute. The samples were typically photoirradiated for five minutes. The irradiated sample was measured below 12 K with ordinary ESR technique in X-band range; resonant microwave frequency was 9.400($\pm$0.004) GHz. The details of ESR and thermoluminescence (TL) measurements were previously reported in Ref. 11. Raising- and lowering-rates of temperature in measuring TL were 0.5 K/s. In pulse-annealing measurement, the sample was kept for about one second at annealing temperature.

PL was induced with the second harmonics (pulsed 5-ns-width, 10-Hz, and 2.33-eV light) generated from a Nd:YAG (yttrium aluminum garnet) laser; the incident light causes exciton-resonant two-photon excitation. The

PL properties are essentially the same as those induc[ed]
under one-photon excitation with UV light ($\hbar\omega \geq$ [4]
eV). The PL was detected with an intensified CCD ca[m]
era with a grating monochromator, and time-resolved [PL]
spectra were measured by gating the CCD camera; t[he]
temporal resolution was 5 ns.

III. EXPERIMENTAL RESULTS

A. ESR Spectra and thermoluminescence

Figure 2 shows typical ESR spectrum measured at 7 [K]
after photoirradiation at 6 K; the ESR signals at 326, 5[22]
1400, and 1480 mT are readily induced together, wh[ile]
the signal at 1180 mT appears even in measuring emp[ty]
capillary. Therefore, as reported in Ref. 25, the signal [at]
1180 mT is ascribed to oxygen molecules in the capilla[ry.]
The photoinduced four signals show similar thermal pr[o-]
file; besides, they saturate for microwave power high[er]
than 0.01 mW below 7 K, while keep linear response [up]
to 0.1 mW at 10 K. Consequently, the four signals a[re]
ascribed to the same origin. The intense ESR signal [at]
326 mT, which is enlarged in the inset, consists of o[ne]
broad resonance with 6-mT width; the structure diff[ers]
from the fivefold split A signal in Fig. 1. The sign[als]
at 326 and 522 mT are almost independent of rotati[on]
angles. Though the two signals around 1400 mT depe[nd]
on rotation angles, they degenerate when the magne[tic]
field vector is parallel to the crystallographic axes. T[he]
reason for the split and the rotation-angle dependence [is]
discussed in Sec. IV A. The intense line at 326 mT w[as]
induced by x-ray irradiation at 10 K and was named as [C]
signal in Ref. 5. The small signal at 336 mT in the ins[et]
of Fig. 2 is the B signal named in Ref. 5; it is far weak[er]
than the C signal and hardly depends on rotation angl[e.]
From now on, we focus on the main signals of the A, t[he]
C, and the satellite signals.

Except for 1180-mT resonance, the ESR spectrum [in]
Fig. 2 is very similar to that of Pb^{3+} in KCl:Pb;[26] ther[e-]
fore, the ESR signals in Fig. 2 are ascribed to hole cente[rs]
of Pb^{3+}. The hole centers are analyzed with spin Hami[l-]
tonian and are compared with Pb^{3+} centers in other ho[st]
crystals in Sec. IV A.

Figure 3 displays the ESR spectra measured at 9 [K]
after photoirradiation at 8, 60, 70, 80 and 90 K. A se[-]
quence of the spectra was measured by carrying out th[e]
photoirradiation and the ESR-data taking alternatel[y.]
The ESR spectra after irradiation at 8–50 K are essen[-]
tially the same in shape. At 60 K, $Pb_2{}^{3+}$ signals becom[e]
prominent, and the signals around 330 mT are compose[d]
of Pb^{3+} signals and other split signals at 60–80 K. Th[e]
Pb^{3+} signals are eventually replaced by the A signal a[t]
90 K.

Figure 4 presents ESR spectrum (lower) after photoi[r-]
radiation at 10 K, namely, before pulse annealing an[d]
ESR spectrum (upper) after pulse annealing at 100 [K.]
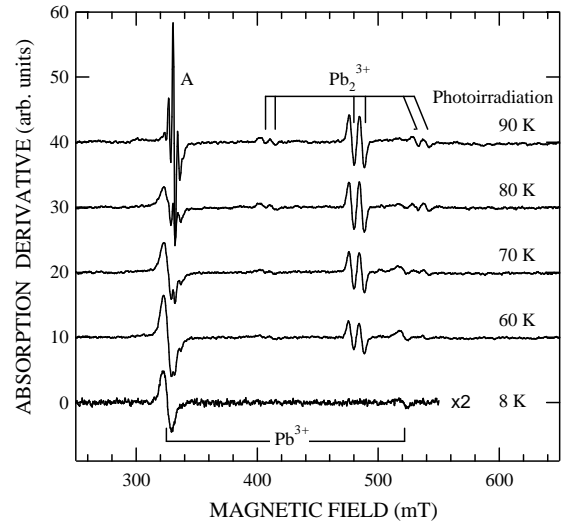Both spectra were measured at 12 K. The ESR spectru[m]

FIG. 3: ESR spectra measured at 9 K after photoirradiation
at various temperatures. They are displayed with the vertical
offset. ESR spectrum at 8 K is enlarged by two times. Mi-
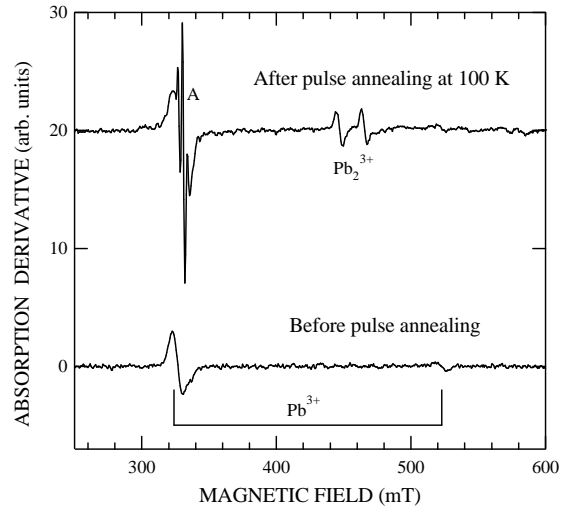crowave frequency was 9.400 GHz. Magnetic field vector **B**

FIG. 4: Photoinduced ESR signals before and after pulse an-
nealing at 100 K. Both spectra were measured at 12 K. Mi-
crowave frequency was 9.400 GHz. Magnetic field vector **B**
was the bc plane; the angle between the **B** and the b axis was
$40°$.

before pulse annealing has the two prominent signals at
326 and 522 mT, which come from Pb^{3+} centers. In the
spectrum after pulse annealing, the signals from STEL
centers of $Pb_2{}^{3+}$ appear around 460 mT, the A signal is
observed around 330 mT, and the residual signal from
Pb^{3+} centers is still detected in the low-magnetic-field
side of the A signal.

Figure 5 shows TL-growth curve (solid line) and the
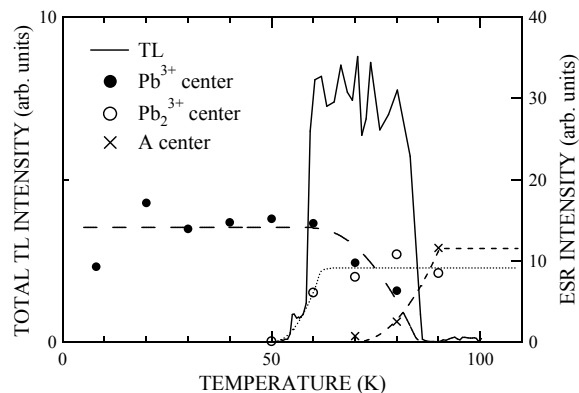intensity of ESR signals in Fig. 3 (open and closed circles

FIG. 5: TL-growth curve (solid line) measured with rais[...]
temperature at 0.5 K/s. ESR intensity in Fig. 3 is shown [...]
comparison; Pb^{3+} (closed circle), Pb_2^{3+} (open circle), and [...]
centers (cross). Dashed, dotted, and broken lines are dra[...]
for guides to the eye.

and cross). TL is observed strongly at 60–85 K un[...]
the condition of raising temperature at 0.5 K/s. The [...]
spectrum in the temperature range is in agreement w[...]
the BG-PL spectrum.

In a previous TL experiment,[15] TL-growth curve m[...]
sured with raising temperature at 0.1 K/s shows two d[...]
crete peaks at 51 and 74 K. The difference probably [...]
sults from the temperature-rising rate; the rising r[...]
in the previous report is slower than that in our me[...]
surement. The discrete peaks suggest the two differe[...]
thermal activation in 50–80 K. The two thermal transf[...]
were assigned to hole activation in Ref. 15. We disc[...]
the activated carriers in Sec. IV B.

B. Photoluminescence

Figure 6 presents PL spectra under exciton-reson[...]
two-photon excitation at 4.66 eV. The PL spectra at 6–70
K are peaked at 2.52 eV and almost invariant in shape.
Above 70 K, the PL spectrum begins to move toward
high-energy side, and the peak reaches 2.7 eV at 100 K.
In the range above 100 K, low-energy PL around 2 eV
relatively increases with raising temperature, and finally
the PL spectrum consists of broad PL bands at 150 K.
The thermal behavior of PL induced under one-photon
excitation into the fundamental absorption region ($\hbar\omega \geq$
4.8 eV) is the same as that in Fig. 6.

Figure 7 shows PL spectra (solid line) and time-
resolved PL (TRPL) spectra (dashed and dotted lines)
under two-photon excitation at 4.66 eV, measured at 6,
75, and 90 K. The dashed line at 6 K represents the BG-
PL band at 2.50 eV; the spectrum is obtained by mea-
suring the PL over 1–99 ms, that is, by gating the CCD
camera with 1-ms delay and 98-ms width. The BG-PL
band decays phosphorescently; the intensity $I(t)$ is well
described by $I(t) = (K/t)[1 - \exp(-t/\tau)]$ where K is a
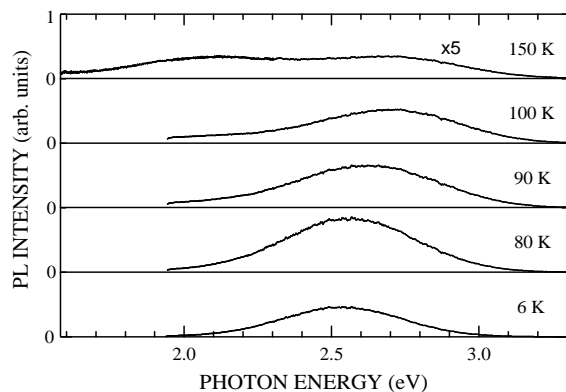proportionality constant and $\tau = 100$ μs.[19] The rest of

FIG. 6: PL spectra at 6, 80, 90, 100, and 150 K under exciton-
resonant two-photon excitation at 4.66 eV. PL spectrum at
150 K is enlarged by five times.

the PL at 6 K is the PL band at 2.66 eV (arrow) and de-
cays single-exponentially with 5.0 μs. This blue PL band
is different from the blue PL band at 2.88 eV mentioned
in Sec. I; the blue PL band at 2.88 eV is not induced un-
der the present excitation. The PL spectra at 75 and 90
K are spectrally resolved with the TRPL spectra peaked
at 2.79 eV (arrow). The blue PL band at 2.79 eV decays
single-exponentially with 2.6 μs at 75 K. Thus, the rela-
tive increase of the blue PL band results in the apparent
high-energy shift of the PL spectrum in Fig. 6.

PL intensity integrated over 2.0–3.2 eV at 6–200 K is
plotted against temperature in Fig. 8; time-integrated
PL intensity over 0–99 ms is represented with cross, and
TRPL intensity over 1–99 ms with closed circle. PL in-
tensity keeps almost constant below 50 K and increases
in 50–70 K. The increase is coincident with TL growth
(dotted line), and the peaks of PL and TRPL intensity
are located at about 80 K. Because the TRPL intensity
corresponds to the phosphorescent component of PL, the
increase of the PL intensity is ascribed to that of the
phosphorescent BG-PL. Indeed, PL at 75 K decays in
proportional to t^{-1} for $t \geq 1$ ms. The TRPL intensity
decreases in 80–100 K and is hardly observed above 100
K. The TRPL quenching is also coincident with the high-
energy shift due to the relative increase of the blue PL
band at 2.79 eV as shown in Fig. 7. Thus, the phospho-
rescent BG-PL band is induced below 100 K. Above 100
K, the blue PL band and other PL band around 2 eV are
dominantly induced and are finally quenched around 200
K.

IV. DISCUSSION

A. Spin-Hamiltonian analysis of self-trapping hole centers

The ESR signals at 326, 522, and about 1400 mT in
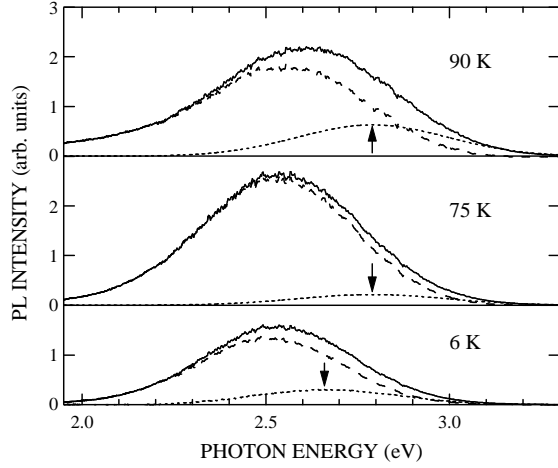Fig. 2 show the same temperature profile and the inten-

FIG. 7: PL (solid line) and time-resolved PL (dashed a dotted lines) spectra at 6, 75 and 90 K under two-pho excitation at 4.66 eV. PL in μs range corresponds to blue (dotted line), and the rest of PL does to phosphorescent bl green PL band (dashed line). Arrows indicate the blue-peaks, and are located at 2.66 eV for 6 K and at 2.79 eV 75 and 90 K.

sity ratio (326 mT) : (522 mT + 1400 mT) = 8 : 2. T ratio is consistent with the isotope ratio of Pb ions; th have two isotope series such as $I = 0$ and $1/2$, and t natural ratio is about 8 : 2. If the intense signal at 3 mT corresponds to Zeeman transition, the g value is es mated to be 2.06; the value larger than the free-electro value of 2.0023 implies that the center is a hole center Indeed, from the comparison with Pb^{3+} in KCl:Pb,[26] t ESR signals are ascribed to hole centers of Pb^{3+}. T spin Hamiltonian $\mathcal{H}$ of the hole center is given by

$$\mathcal{H} = \mu_B \mathbf{B} \cdot \underline{g} \cdot \mathbf{S} + \mathbf{S} \cdot \underline{A} \cdot \mathbf{I} - \mu_n \mathbf{B} \cdot \underline{g}_N \cdot \mathbf{I}, \qquad (1)$$

where μ_B denotes the Bohr magneton, $\mathbf{B}$ magnetic field vector, $\underline{g}$ the Zeeman tensor, $\mathbf{S}$ the electron spin, $\underline{A}$ the hyperfine tensor, μ_n the nuclear magneton of ^{207}Pb ($\mu_n = 0.5892\mu_N$, μ_N: the nuclear magneton), $\mathbf{I}$ the nuclear spin, and $\underline{g}_N$ the nuclear Zeeman tensor. We note that the first-order hyperfine interaction of the hole with surrounding Cl-nuclei is not included in the Hamiltonian because our experimental results give no evidence of the superhyperfine (SHF) effect that the interaction splits each resonance at 326, 522, and 1400 mT in Fig. 2 into tens of fine resonances as observed in PbF_2 (Ref. 10). Equation (1) describes the center that a hole strongly localizes on a Pb^{2+} ion, namely, self-trapping hole center of Pb^{3+}.

Equation (1) for $I = 0$ is reduced to the electron Zeeman term. The intense signal at 326 mT in Fig. 2 slightly depends on rotation angles. Spin Hamiltonian analysis for the Zeeman transition provides principal g values as shown in Table I; we set $x = c$, $y = b$, and $z = a$ in this analysis.

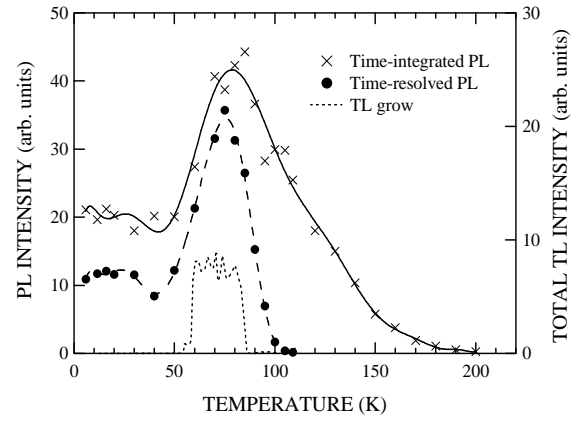In analyzing the spin Hamiltonian for $I = 1/2$, we can

FIG. 8: PL intensity integrated over 2.0–3.2 eV vs temperature; cross denotes time-integrated PL intensity over 0–99 ms and closed circle stands for time-resolved PL intensity over 1–99 ms. Solid and dashed lines are drawn with polynomial functions for guides to the eye. TL-growth curve (dotted line) is also presented for comparison.

TABLE I: Principal g and A values of spin Hamiltonian [Eq. (1)]. The parameters of Pb^{3+} centers in other host crystals are cited for comparison. The A values are represented in GHz.

Host of Pb^{3+}	g values			A values
	g_x	g_y	g_z	(GHz)
$PbCl_2$[a]	2.044	2.062	2.044	26.7
	± 0.001	± 0.001	± 0.001	± 0.4
KCl:Pb[b]		2.034 ± 0.001		33.0 ± 0.1
ThO_2:Pb[c]		1.967 ± 0.001		36.8 ± 0.2
ZeSe:Pb[d]		2.072 ± 0.001		20.7 ± 0.1
ZeTe:Pb[e]		2.167		15.7

[a]This work.
[b]Reference 26; g tensor is assumed to be isotropic.
[c]References 28 and 29.
[d]Reference 30.
[e]Reference 31; the accuracy of g and A velues is not reported.

assume that the A tensor is isotropic because the resonance at 522 mT is independent of rotation angles. Furthermore, we replace, for simplicity, the contribution of nuclear Zeeman term to the energy eigenvalues with the effective nuclear g_N value along the corresponding magnetic field. The simplification is justified because the contribution of the nuclear Zeeman term to Eq. (1) is small enough; indeed, the resonances are described by the electron Zeeman and isotropic hyperfine terms in a good approximation. Pb^{3+} centers in other host crystals[26,28,29,30,31] were analyzed within this approximation. However, to estimate g_N values, we choose to include the effective value into the energy eigenvalues. The obtained equations of the eigenvalues are the same as Breit-Rabi formula,[32] which was applied to Pb^{3+} centers in other hosts.[26,28,29,30,31] Figure 9 depicts energy diagram of Eq.
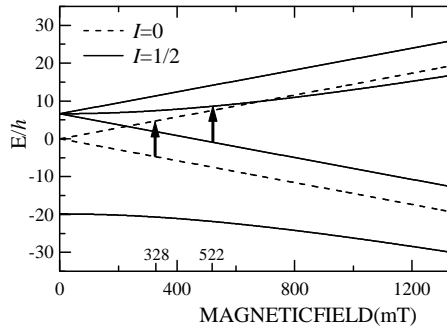
FIG. 9: Energy diagram of spin Hamiltoni[...]
$\mathbf{B} \parallel a$. Broken lines: energy levels for I [...]
electron Zeeman levels. Solid lines: energy lev[...]
Arrows stand for observed ESR transitions at [...]
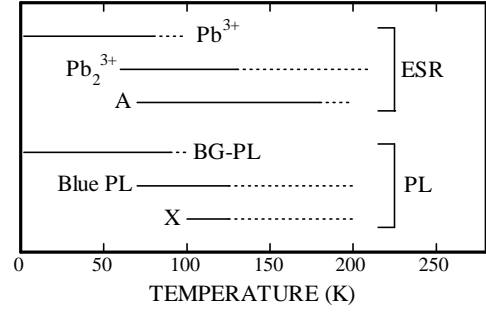ordinate is represented in GHz.

FIG. 10: Schematic diagram for thermal stability of the photoinduced ESR signals and PL bands. Solid line: the stable range of the signals. Dotted line: the unstable but still detectable range. Blue PL denotes the blue PL band at 2.79 eV in Fig. 7. X stands for the broad PL band around 2.1 eV in Fig. 6

(1) for $\mathbf{B} \parallel a$; broken lines denote energy l[...]
and solid lines for $I = 1/2$. Arrows in Fig. [...]
ESR transitions observed in the measure[...]
ical estimation on g_N gives the values be[...]
6 for various directions of $\mathbf{B}$. The anisot[...]
tensor is responsible for the rotation-angle[...]
the ESR signals around 1400 mT; moreove[...]
angle dependence indicates the deviation [...]
axes from the a, b, and c axes. In the uni[...]
crystal, there exist two-equivalent Pb-ion[...]
flect the crystallographic symmetry. The [...]
around 1400 mT in Fig. 2 are explained b[...]
sible configurations of Pb^{3+} centers in th[...]
by the anisotropy of the g_N tensor.

The evaluated g and A values are lis[...]
together with the g and A values of Pb^{3+} [...]
hosts. The g values are about 2 in all hos[...]
values vary in 16–37 GHz. The A values [...]
spatial spread of the hole is quite differen[...]

B. Thermal stability of ESR signals a[...]

Below 70 K holes localize on Pb^{2+} ions and form self-trapping hole centers of Pb^{3+}, and, on the other hand, electron centers are not detected at 0–1700 mT below 50 K. As STEL centers with simple configuration, monomer Pb^+ and dimer Pb_2^{3+} centers are possible in $PbCl_2$. Indeed, Pb_2^{3+} centers are observed above 60 K. Pb^+ centers usually have g value of 1.0–1.6 in Pb-doped alkali chloride;[33] in our measurement, the ESR signal would appear at 400–700 mT if it exists. However, the STEL centers of Pb^+ have not been detected. Thus, it is improbable that the Pb^+ centers are induced in $PbCl_2$.

The sharp TL growth at 55 K in Fig. 5 indicates the thermal activation of trapped carriers. Because the STEL centers of Pb_2^{3+} appear at 60 K and the hole centers of Pb^{3+} are quite stable at 60 K as shown in Fig. 3, the activated carriers at 55 K are ascribed to electrons. However, the trapped state of electrons below 50 K has

not been observed at 0–1700 mT. The electron center is most likely to has either of the following structures; (i) the center with ESR in the region higher than 1700 mT, or (ii) the center without ESR. We discuss in Sec. IV D the relaxation dynamics of electrons below 50 K, producing the trapped state.

The ESR spectra in Fig. 3 show that Pb^{3+} centers thermally change into the A center above 70 K and are finally replaced at 90 K. In a pulse-annealing experiment[34] on PbCl:Tl, the A signal is weaken under annealing at 200 K, and the ESR signals coming from hole-trapping centers of Tl^{2+} grow at the temperature. The result implies that the A signal originates from hole-trapping centers. The STEL centers of Pb_2^{3+} appear above 60 K as shown in Figs. 3 and 4, become unstable thermally above 130 K, and are quenched around 210 K.[8,34]

Figure 10 summarizes and schematically represents the thermal stability of ESR signals and PL bands; solid lines stand for the stable range, and dotted lines denote unstable but still detectable range. Blue PL in Fig. 10 denotes the blue PL band at 2.79 eV in Fig. 7, and X does the broad PL band around 2 eV in Fig. 6. Obviously, the BG-PL band is thermally coincident with the STH centers of Pb^{3+}. In addition, the thermal activation of electrons at 55 K corresponds to the TL which has the same shape with the BG-PL band. Consequently, we ascribe the luminescent state yielding the BG-PL band to the STE associated with a Pb^{3+} center; probably, the STE has the configuration of (Pb^{3+} + electron). The disagreement of the BG-PL band with Pb_2^{3+} centers in Fig. 10 excludes the model for the BG-PL band proposed in Refs. 15,16,17,18.[40] The blue PL band at 2.79 eV almost corresponds to the STEL centers of Pb_2^{3+} and the A centers. Therefore, this study provides a possibility that the blue PL band comes from the STE's associated with Pb_2^{3+} centers, but, to identify the origin, the further study with optically detected magnetic resonance technique is surely needed.

C. Origin of "A signal"

The origin of the A signal has been disputed over the past three decades; it was once attributed to electron centers of Pb^+ (Refs. 5 and 6), but the properties of the A signal, the g value and the ESR spectrum, are far different from those of Pb^+ in other host crystals.[7]

The A signal was recently assigned to self-trapping hole centers of Cl_2^- (V_K centers).[34] The A signal is composed of five resonances as presented in Fig. 1; the intensity ratio at 9 K is estimated to be $1 : 10 : 27 : 10 : 0.5$. However, the ESR spectrum of Cl_2^- splits into seven resonances in the first-order hyperfine effect, and the intensity ratio of $1 : 2 : 3 : 4 : 3 : 2 : 1$ disagrees with that of the A signal. Moreover, the rotation-angle dependence of the A signal[5] does not show the anisotropy peculiar to the dimer-molecular V_K centers,[3] but is almost isotropic. Thus, the A signal is unlikely to originate from the V_K-type hole centers of Cl_2^-.

Furthermore, the A signal of five resonances does not come from the Pb^{3+} centers with SHF interaction as observed in PbF_2 (Ref. 10), because (i) the satellite at 522 mT disappears up to 90 K as shown in Fig. 3 and (ii) the SHF structure, which stems from the interaction of the Pb^{3+} centers with the surrounding Cl^- ions, is composed of tens of fine resonances.[26]

As shown in Fig. 4, the A signal appears under pulse annealing at 100 K after photoirradiated at 10 K. This result indicates that the localized state responsible for the A signal is produced by thermal transfer of the localized states induced at 10 K. In addition, Fig. 3 shows that the STEL centers of Pb_2^{3+} are stable over 80–90 K where the Pb^{3+} signals change into the A signal. Consequently, we declare that the A signal is formed by either of the two following ways: (i) The STH centers become unstable around 80 K and the holes transfer to other trapped state associated with permanent lattice defects. (ii) Vacancies begin to move thermally around 70 K, affect the STH centers, and modify the STH centers or make the STH center unstable. In any way, the A signal is ascribed to the hole-trapping centers associated with the permanent lattice defects such as vacancies or impurities or both.

D. Relaxation dynamics of electron-hole pairs

We discuss here the relaxation of e-h pairs in $PbCl_2$ from the comparison with relaxation in $PbBr_2$ (Ref. 24).

In $PbBr_2$, the spontaneous dissociation of e-h pairs was reported,[24] and the individual self-trapped states of both electrons and holes have been recently evidenced with ESR technique.[11]

However, the present ESR study on $PbCl_2$ shows that the relaxed states of e-h pairs are STH's and trapped electrons below 50 K, STH's and STEL's at 60–70 K, and the A centers and STEL's at 80–130 K (Fig. 10). The complicated results probably come from the inevitably dense vacancies in $PbCl_2$;[35,36] $PbCl_2$ crystals are high-ionic conductors and therefore include dense anion vacancies more than 10^{17} cm^{-3}. In the crystals, the anion vacancies or the vacancy-associated defects are electron traps and can be competitors to the STEL centers of Pb_2^{3+}. Indeed, the thermal production of the STEL's in Fig. 4 suggests that the competitors are efficient enough to result in the absence of STEL's below 50 K.

According to the theoretical study by Sumi,[37] the exciton–acoustic-phonon interaction determines the relaxed state of e-h pairs and classifies the relaxed states by the strength and the sign of the coupling constants. In the theoretical study, the crystallographic field is idealized with omitting the lattice defects such as dense vacancy, so that the study is not applicable to $PbCl_2$ straightforwardly. However, the coexistence of STEL's and STH's at 60–70 K shows the evidence that both electrons and holes strongly interact with acoustic phonons. Consequently, though the localized states are far more complicated in the real crystal, we believe that the e-h relaxation similar to that in $PbBr_2$ does also realize in $PbCl_2$.

At the end of discussion, we compare the relaxed states of e-h pairs in PbF_2, $PbCl_2$, and $PbBr_2$. Though the crystallographic structure of β-PbF_2 is cubic and those of $PbCl_2$ and $PbBr_2$ are orthorhombic,[20] STH centers in β-PbF_2 (Ref. 10) and $PbCl_2$ are monomer Pb^{3+} centers while STH centers in $PbBr_2$ are dimer Br_2^- centers.[11] The relaxed states indicate that holes in β-PbF_2 and $PbCl_2$ strongly interact with Pb^{2+} ions while holes in $PbBr_2$ do with Br^- ions. The top of the valence band in $PbCl_2$ is composed of about half-to-half Pb^{2+} ($6s$) and Cl^- ($3p$),[12] but the holes nevertheless localize only on Pb^{2+} ions. On the other hand, though the bottoms of the conduction band in β-PbF_2, $PbCl_2$, and $PbBr_2$ are composed of the $6p$ states of Pb^{2+} ions,[12,38] electrons in β-PbF_2 do not get self-trapped while electrons in $PbCl_2$ and $PbBr_2$ form STEL centers of Pb_2^{3+}. From the comparisons here, we remark that in lead halides the structure of electronic band does not simply determine the relaxed states of e-h pairs, but the electron-phonon and the hole-phonon interaction plays a crucial role to determine the relaxed states.

V. CONCLUSIONS

We have comprehensively investigated photoinduced ESR signals and PL in a wide range of 5–200 K in $PbCl_2$. As a result, the hole centers below 70 K have been found to be self-trapping centers of Pb^{3+}. The ESR study in the wide temperature range reveals the thermal change of localized centers; in particular, the grow of the STEL centers of Pb_2^{3+} and the thermal transfer from the STH centers to the A centers. From the comparison with the thermal stability of the localized centers, the origins of PL bands have been discussed; we finally conclude that the STH centers of Pb^{3+} are responsible for the STE's yielding the BG-PL band at 2.50 eV.

Acknowledgments

We would like to thank Mr. I. Katayama and Mr. T. Hasegawa for technical assistance in ESR experiments.

[1] Y. Toyozawa, in *Excitonic Processes in Solids,* edited by M. Ueta, H. Kanzaki, K. Kobayashi, Y. Toyozawa, and E. Hanamura (Springer, Berlin, 1986), chap. 4.

[2] K. S. Song and R. T. Williams, *Self-Trapped Excitons* (Springer, Berlin, 1993).

[3] R. H. Silsbee, in *Electron Paramagnetic Resonance,* edited by S. Geschwind (Plenum Press, New York-London, 1972), chap. 7.

[4] J. Arends and J. F. Verwey, Phys. Status Solidi **23**, 137 (1967).

[5] W. C. De Gruijter and J. Kerssen, J. Solid State Chem. **5**, 467 (1972).

[6] J. Kerssen, W. C. De Gruijter, and J. Volger, Physica (Amsterdam) **70**, 375 (1973).

[7] P. G. Baranov and J. Rosa, Solid State Commun. **74**, 647 (1990).

[8] S. V. Nistor, E. Goovaerts, and D. Schoemaker, Phys. Rev. B **48**, 9575 (1993).

[9] T. Hirota, T. Fujita, and Y. Kazumata, Jpn. J. Appl. Phys., Part 1 **32**, 4674 (1993).

[10] M. Nishi, H. Hara, Y. Ueda, and Y. Kazumata, J. Phys. Soc. Jpn. **42**, 1900 (1977).

[11] M. Iwanaga, J. Azuma, M. Shirai, K. Tanaka, and T. Hayashi, Phys. Rev. B **65**, 214306 (2002).

[12] M. Fujita, M. Itoh, Y. Bokumoto, H. Nakagawa, D. L. Alov, and M. Kitaura, Phys. Rev. B **61**, 15731 (2000).

[13] W. C. De Gruijter and T. Bokx, J. Solid State Chem. **6**, 271 (1973).

[14] G. Liidja and Vl. Plekhanov, J. Lumin. **6**, 71 (1973).

[15] M. Kitaura, A. Ohnishi, and M. Itoh, J. Phys. Soc. Jpn. **69**, 2360 (2000).

[16] M. Kitaura and H. Nakagawa, J. Phys. Soc. Jpn. **70**, 2462 (2001), and earlier references cited therein.

[17] S. V. Nistor, M. Stefan, E. Goovaerts, and D. Schoemaker, J. Lumin. **87-89**, 549 (2000).

[18] V. Babin, A. Krasnikov, M. Nikl, A. Stolovits, and S. Zazubovich, Phys. Status Solidi B **229**, 1295 (2002).

[19] M. Iwanaga, M. Watanabe, and T. Hayashi, Int. J. Mod. Phys. B **15**, 3677 (2001).

[20] R. W. G. Wyckoff, *Crystal Structures,* 2nd ed. (Wiley, New York, 1963), vol. 1.

[21] A. F. Malysheva and V. G. Plekhanov, Opt. Spektrosk. **34**, 527 (1973), [Opt. Spectrosc. **34**, 302 (1973)].

[22] A. J. H. Eijkelenkamp and K. Vos, Phys. Status Solidi B **76**, 769 (1976).

[23] J. Kanbe, H. Onuki, and R. Onaka, J. Phys. Soc. Jpn. **43**, 1280 (1977).

[24] M. Iwanaga, M. Watanabe, and T. Hayashi, Phys. Rev. B **62**, 10766 (2000).

[25] H. Kon, J. Am. Chem. Soc. **95**, 1045 (1973).

[26] D. Schoemaker and J. L. Kolopus, Solid State Commun. **8**, 435 (1970).

[27] C. P. Slichter, *Principals of Magnetic Resonance,* 3rd ed. (Springer, Berlin, 1990), chap. 11.

[28] R. Röhrig and J. Schneider, Phys. Lett. **30A**, 371 (1969).

[29] J. L. Kolopus, C. B. Finch, and M. M. Abraham, Phys. Rev. B **2**, 2040 (1970).

[30] K. Suto and M. Aoki, J. Phys. Soc. Jpn. **26**, 287 (1969).

[31] K. Suto and M. Aoki, J. Phys. Soc. Jpn. **24**, 955 (1968).

[32] G. Breit and I. I. Rabi, Phys. Rev. **38**, 2082 (1931).

[33] E. Goovaerts, S. V. Nistor, and D. Schoemaker, Phys. Rev. B **28**, 3712 (1983).

[34] S. V. Nistor, E. Goovaerts, M. Stefan, and D. Schoemaker, Nucl. Instrum. Methods Phys. Res. B **141**, 538 (1998).

[35] J. F. Verwey and J. Schoonman, Physica (Amsterdam) **35**, 386 (1967).

[36] J. Oberschmidt and D. Lazarus, Phys. Rev. B **21**, 5813 (1980).

[37] A. Sumi, J. Phys. Soc. Jpn. **43**, 1286 (1977).

[38] M. Nizam, Y. Bouteiller, B. Silvl, C. Pisani, M. Causa, and R. Dovesi, J. Phys. C **21**, 5351 (1988).

[39] Another PL band at 1.8–1.9 eV was reported. Because it is mainly induced under excitation into the low-energy range of the fundamental absorption including exciton absorption (Refs. 5,13 and 16), the PL band is unlikely to be intrinsic PL. Therefore, the PL band is not discussed in this paper.

[40] From the experimental evidence presented already, we can also discuss the models for the UV-PL and 2.88-eV blue-PL bands in Refs. 15,16,17,18; the absence of Pb^+ centers denies the model in Refs. 15,16,17, and the disagreement of the temperature range of Pb_2^{3+} centers with those of the UV-PL and blue-PL bands excludes the model in Ref. 18.